Strong edge burst with bipolar non-Hermitian skin effect

C. Yuce* and H. Ramezani
Department of Physics, Eskisehir Technical University, 26555 Eskisehir, Turkey
and Department of Physics and Astronomy, University of Texas Rio Grande Valley, Edinburg, Texas 78539, USA

(Received 15 February 2024; revised 8 April 2024; accepted 14 May 2024; published 6 June 2024)

We consider a system exhibiting the bipolar non-Hermitian skin effect (NHSE), where bipolar skin states are localized at both edges, and discuss how the topological funneling effect can occur with a single focal point in this system. We explore a topological phase transition from bipolar NHSE to NHSE, which alters the localization characteristics of the eigenstates. After the transition, both the delocalized and bipolar skin states transform into skin states. The non-Hermitian edge burst is a novel and unexpected feature of non-Hermitian quantum dynamics, characterized by substantial particle loss at the boundary of a system. Using the model displaying bipolar NHSE, we show the emergence of the edge-burst effect with a large amount of loss observed only at one boundary. To enhance this effect, we introduce slightly asymmetric long-range couplings into a system that already exhibits the edge burst. This leads to a notable enhancement of the edge burst. We discuss the significance of asymmetrical local power generation in contributing to this enhanced edge-burst effect.

DOI: 10.1103/PhysRevB.109.214301

I. INTRODUCTION

Non-Hermitian systems display intriguing and unique topological properties not found in their Hermitian counterparts. A noteworthy phenomenon in non-Hermitian systems is the non-Hermitian skin effect (NHSE), where the eigenstates and eigenvalues exhibit high sensitivity on the boundary conditions, challenging the conventional understanding of bulk-boundary correspondence [1–5]. The NHSE describes a unique non-Hermitian phenomenon where all eigenstates under open boundary conditions (OBCs) are localized near the boundary, while those under periodic boundary conditions (PBCs) are extended. Studies have revealed that the emergence of the NHSE in one dimension is linked to the spectral winding number, a topological invariant unique to non-Hermitian systems [6–8]. Recently, there has been significant attention on the bipolar NHSE, which occurs in non-Hermitian systems when long-range coupling is introduced [9–18]. Unlike conventional NHSE, where skin states asymmetrically localize at one edge, bipolar NHSE implies that skin modes appeared either at the left or the right edge. The spectral characteristics of NHSE continue to be a significant subject of investigation within the non-Hermitian community due to its unconventional implications and promising potential applications in different fields.

The NHSE also leads to intriguing dynamical effects such as topological funneling [19–21] and edge-burst effects [22–26]. Non-Hermitian topological funneling, observed in the context of light propagation in photonic lattices, relies on NHSE, channeling light to a focal point regardless of its initial form. In recent years, a new phenomenon called the non-Hermitian edge burst has captured the interest of researchers. The non-Hermitian edge burst refers to a significant portion of loss occurring at the system boundary. Understanding and characterizing the non-Hermitian edge burst is crucial for both fundamental research and technological applications. Originally, the edge burst was attributed to topological edge states [22], which is questioned in a paper [23]. Its physical origin is found to be an interplay between two unique non-Hermitian phenomena: the NHSE and imaginary gap closing [23]. However, recent work has emphasized that while these conditions can give rise to the edge burst, they are not necessary and sufficient for the emergence of the edge-burst effect [24]. It was shown that this effect appears even in a particular one-dimensional lossy lattice with nonuniform loss rates, where the skin localization is absent. Experimental observations by Xue's group, using single-photon discrete-time quantum walks, have confirmed the existence of the edge-burst effect [26].

To date, studies of the edge-burst effect have primarily focused on lossy non-Hermitian systems without considering asymmetrical couplings. Our paper aims to investigate the non-Hermitian edge burst in a lattice with asymmetrical long-range couplings, exhibiting bipolar NHSE. We will explore the underlying mechanisms and their properties using theoretical and numerical methods, analyzing system behavior, time evolution, local decay distribution, and sensitivity to parameters. Our focus will be on how the edge-burst effect enhances with asymmetrical couplings, leading to nonexponential decay of total power from the system. Additionally, we will discuss the topological funneling effect in the context of bipolar NHSE. This paper contributes to expanding knowledge on the edge-burst effect in non-Hermitian systems.

II. BIPOLAR NHSE

Tight-binding lattices with asymmetric couplings between nearest-neighboring sites serve as prominent systems in the field of non-Hermitian systems, providing insights into the

*cyuce@eskisehir.edu.tr

 ©2024 American Physical Society

behavior of nonreciprocal systems and their topological properties. In this paper, we explore a modification of this model, wherein the asymmetry is introduced not in the couplings between nearest-neighboring sites, but rather between the next-to-nearest neighboring sites. Furthermore, we consider the presence of losses at each odd-numbered site within the lattice [Fig. 1(a)]. Therefore, the non-Hermitian character arises from both the losses and the asymmetry between the forward and backward long-range couplings in the system. This minimal model serves as the basis for our investigation on the non-Hermitian edge burst. The equation for the field amplitude ψ_j at site $j = 1, 2, \ldots, N$ reads

$$\psi_{j+1} + \psi_{j-1} + i(\gamma_L\, \psi_{j+2} - \gamma_R\, \psi_{j-2}) - i\, V_j\, \psi_j = i\frac{d\psi_j}{dt}, \tag{1}$$

where $0 \leqslant \gamma_R < 1$ and $0 \leqslant \gamma_L < 1$ are real-valued coefficients in the backward and forward directions, respectively. Therefore, the next-to-nearest-neighboring couplings are purely imaginary, and with a phase difference between the forward and backward directions. The loss rates $V_j > 0$ are nonzero only at odd-numbered sites, i.e., $V_j = V$ when j is odd and $V_j = 0$ when j is even.

We start to study the stationary solutions of Eq. (1). The PBC eigenvalues can be readily found in closed analytical form using the k-space Hamiltonian $\mathcal{H} = \begin{pmatrix} i(\gamma_L e^{ik} - \gamma_R e^{-ik}) - iV & 1 + e^{-ik} \\ 1 + e^{ik} & i(\gamma_L e^{ik} - \gamma_R e^{-ik}) \end{pmatrix}$. They are given by

$$E_{\mp}(k) = -(\gamma_R + \gamma_L)\, \sin(k) + i(\gamma_L - \gamma_R)\, \cos(k) - i\frac{V}{2} \mp \sqrt{2 - \frac{V^2}{4} + 2\cos(k)}. \tag{2}$$

This formula allows us to study the topological properties of the system through the spectral winding number for a complex reference energy E_0 [6,8,10],

$$\nu = \int_0^{2\pi} \frac{dk}{2\pi i} \frac{d}{dk} \ln[E(k) - E_0]. \tag{3}$$

The system is topologically nontrivial and demonstrates a strong dependence on the boundary conditions even when $\gamma_R = \gamma_L$, indicating the presence of a skin effect that is not exclusively linked to the asymmetry in the couplings. In other words, the skin states do not require asymmetric couplings in this case, where the non-Hermiticity is only due to losses. To be more precise, the system displays bipolar NHSE, implying localization on both edges. To explore the OBC and PBC spectra on the complex energy plane when $\gamma_R = \gamma_L$, we perform numerical computations in three distinct phases: $V < 4$, $V = 4$, and $V > 4$ [the expression inside the square root in Eq. (2) is always negative]. First, we start with the case when $V < 4$. In this regime, the PBC eigenvalues unveil a distinctive structure characterized by a line almost parallel to the E_R axis and a loop, as depicted in Fig. 1(b). A segment of this line bisects the loop, resulting in two loops with opposite winding numbers $\nu = \mp 1$ that intersect along the line, which we refer to as a *Bloch line*. The OBC modes with eigenvalues inside the loops are identified as skin states. Intriguingly, the skin states exhibit bipolar nature, with eigenvalues in the lower and upper PBC loops localized at the opposite edge. Conversely, the remaining OBC states with the eigenvalues lying on the

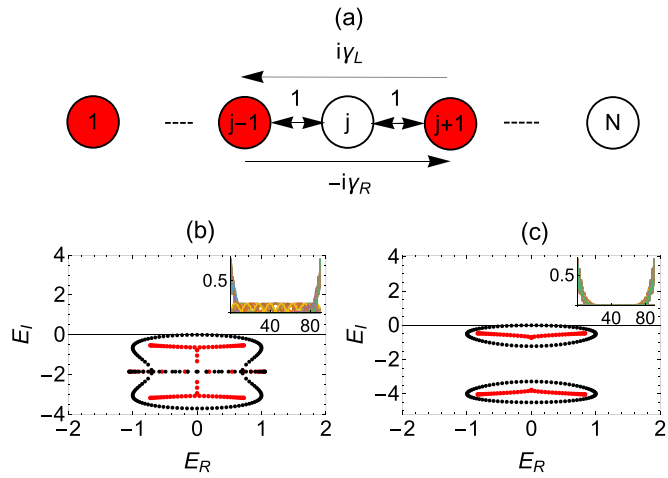

FIG. 1. (a) A schematic of the non-Hermitian model. The lattice sites are colored red and white to represent odd-numbered and even-numbered sites, respectively, with red indicating lossy sites and white representing lossless sites. The numerically computed PBC (black) and OBC (red) spectra in the complex energy plane at $\gamma_R = \gamma_L = 0.5$ and $N = 90$, where the non-Hermiticity arises solely from losses at (b) $V = 3.7$ and (c) $V = 4.5$. The insets are the densities $|\psi_j|^2$ of all OBC eigenstates. The system exhibits bipolar NHSE, with the skin modes being localized at opposite edges ($\nu = 1$ and $\nu = -1$ for the upper and lower loops, respectively). (a) Two loops intersect along the Bloch line whose length decreases with increasing V. Note that the Bloch line eventually transforms into a Bloch point when $V = 4$. (b) The Bloch point vanishes and imaginary line gap occurs when $V > 4$.

line are extended; their eigenvalues display substantial overlap with the corresponding PBC eigenvalues. Therefore, the system under OBC demonstrates a coexistence of extended and bipolarly localized eigenstates. The number of extended states exceeds that of skin states for small values of V. Note that the length of the Bloch line decreases with increasing V, leading to more skin states and less extended states. At the critical loss rate $V = 4$, the Bloch line becomes a Bloch point. Finally, we consider that V exceeds the critical value, $V > 4$, where an imaginary line gap arises on the PBC spectrum. Two distinct PBC loops with opposite windings encircle the OBC eigenvalues [Fig. 1(c)]. The corresponding OBC modes in the upper and lower loops are localized at opposite edges. As V further increases, the PBC loops become more elongated along the E_R axis. If V is exceedingly large, the PBC loops become so elongated that it leads to a substantial overlap with the OBC spectra, meaning that the localization lengths of the OBC states become almost equal to the lattice size. Note that the upper PBC loop touches the E_R axis (a zero-energy PBC eigenstate exists), hence the imaginary gap closing occurs in these three regimes.

Next, we consider the case of the asymmetrical couplings with $\gamma_L > \gamma_R$, where the imaginary gap closing does not occur. In this case, NHSE or bipolar NHSE occurs in the system. In the absence of losses, $V = 0$, where the asymmetry in the couplings is the only source of the non-Hermiticity, the system displays NHSE with the skin states being localized at the left edge. Figure 2(a) illustrates the PBC spectrum according to Eq. (2), consisting of two identical loops with the same

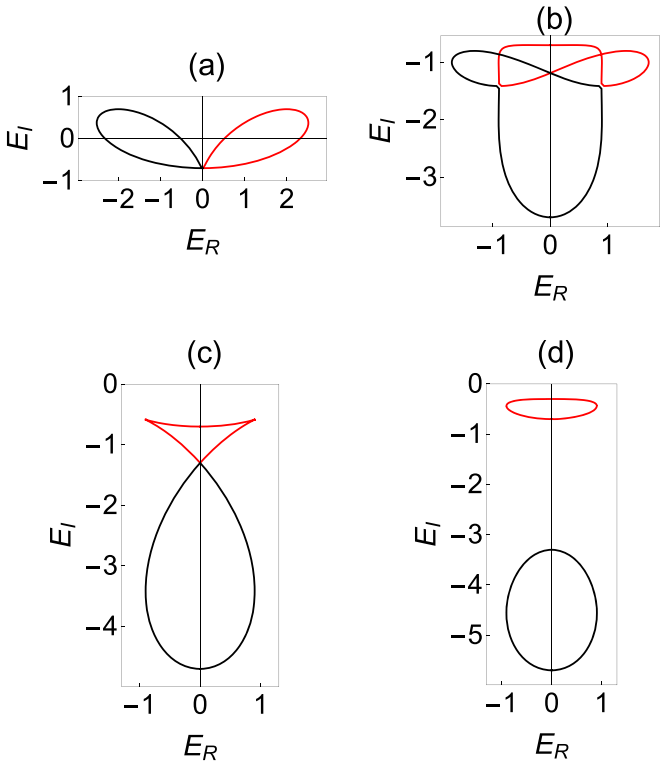

FIG. 2. The PBC spectra $E_{\mp}$ on the complex energy plane according to Eq. (2) at (a) $V = 0$, (b) $V = 3$, (c) $V = 4$, and (d) $V = 5$. The parameters are $\gamma_L = 0.8$, $\gamma_R = 0.1$. The NHSE occurs as both loops have the same windings $\nu = 1$ for (a) and (d), implying skin localization at the left edge. On the other hand, the bipolar NHSE occurs for (b) and (c). (b) The lower loop (in black) has one loop with $\nu = 1$, whereas the upper loop (in red) has two loops with opposite windings $\nu = \mp 1$. (c) The lower and upper loops have opposite windings with $\nu = -1$ and $\nu = 1$, respectively.

winding number $\nu = 1$, implying the existence of the NHSE. The two loops meet at the Bloch point. In the presence of the losses, $V > 0$, the system can exhibit either NHSE or bipolar NHSE, depending on the parameters. Furthermore, the PBC loops are not identical in appearance, with the lower loop having a larger area, as illustrated in Figs. 2(b)– 2(d). The shapes of the loops change significantly depending on whether V is below or above the critical value of 4. For example, the upper red loop is composed of two loops with opposite windings $\nu = \mp 1$, while the lower one has only one loop with $\nu = 1$ when V is below than the critical number [see Fig. 2(b)]. Since $\nu = 1$ and $\nu = -1$ imply the existence of skin states localized at the left and right edge, respectively, we can say that the skin states with eigenvalues in the lower loop are localized at the left edge, while those with eigenvalues in the upper red loop are localized at both edges. Consequently, the skin states localized at the left edge outnumber those at the right edge. At $V = 4$ [see Fig. 2(c)], two nonidentical loops with opposite windings meet at the Bloch point. Notably, the nonidentical nature of the loops also implies differences in localization lengths of the skin states on each edge. If V exceeds 4, an imaginary line gap appears [see Fig. 2(d)]. In this case, an intriguing phase transition occurs from the bipolar NHSE to the NHSE. In Fig. 3, a basic illustration demonstrates such

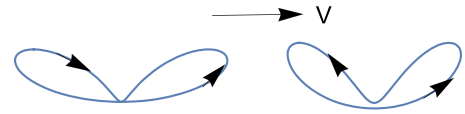

FIG. 3. An illustration of the phase transition from bipolar NHSE to NHSE as the parameter V increases. The two PBC loops with opposite winding numbers, meeting at the Bloch point, change into a single PBC loop with a single winding number. The Bloch point disappears with the phase transition. Under OBC, the system with bipolar NHSE can accommodate skin states localized at both edges and may also have extended states, whereas in the NHSE regime, skin states are asymmetrically localized at one edge. In other words, a slight increase in the parameter V at the transition point shifts all right-localized skin states, along with the extended states, to become left-localized skin states. Note that in the system depicted in Fig. 2(d), the winding number of the lower loop remains unchanged as V crosses the transition point.

a topological phase transition. Physically, a tiny amount of change of V at the transition point can change the localization properties of the eigenstates. This is different from the Hermitian Anderson transition, where even a tiny amount of disorder can localize all extended states. In our system, the OBC system exhibits both delocalized states and bipolar skin states before the phase transition, $V \leqslant V_t$. However, all these states transform into skin states localized at the left edge after the transition takes place. Let us calculate the transition point $V = V_t$ using Eq. (2) when the system has an imaginary line gap. Before the transition occurs, the two Bloch points traverse through the k space, eventually meeting at $k = 0$ at the transition point. If we set $E_+(k = 0) = E_+(k = \pi)$, we obtain the transition point, marking the onset of the NHSE,

$$V_t = \frac{2[1 + (\gamma_L - \gamma_R)^2]}{|\gamma_L - \gamma_R|}. \tag{4}$$

We see that $V_t \to \infty$ if the system has symmetrical couplings, $\gamma_R = \gamma_L$. Note that the transition point is not smaller than the critical point, $V_t \geqslant 4$. As an example, $V_t = 4.25$ for the parameters used in Fig. 2(d). Therefore, the upper loop has the same winding as the lower one in Fig. 2(d), indicating the absence of bipolar NHSE, and all the corresponding skin states are localized only at the left edge.

Topological funneling effect

The NHSE gives rise to intriguing dynamical effects, such as the topological funneling effect—a phenomenon where an arbitrary initial excitation, typically localized at a specific site within the system, always moves towards the focal point where the skin localization occurs, and remains localized at that point [19]. Considering the funneling effect in the dynamics of NHSE, one may ask similar questions about bipolar NHSE, where the skin states exhibit localization near both edges. One might intuitively expect a topological funneling effect with two focal points in the context of bipolar NHSE. In other words, an initial single-site excitation propagates towards both edges by splitting into two distinct wave packets and remains localized there instead of being reflected from the edges. Contrary to this expectation, the initial excitation

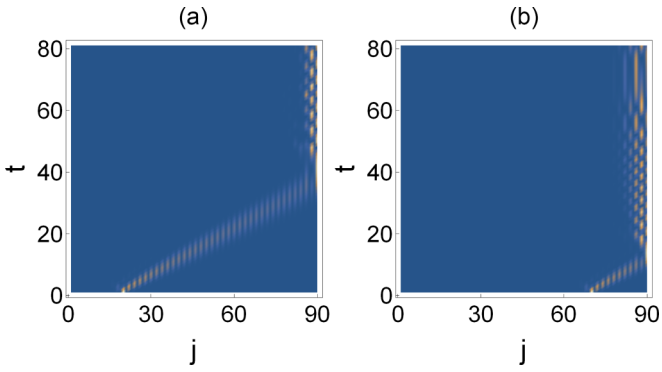

FIG. 4. $\frac{\psi_j(t)}{\sum_j |\psi_j(t)|^2}$ as a function of time with (a) $\psi_j(0) = \delta_{j,20}$ and (b) $\psi_j(0) = \delta_{j,70}$. The lattice has symmetric couplings but is subject to losses at every odd-numbered site. The initial excitation always moves to the right even if the system has bipolar NHSE, where half of the eigenstates are localized at the left edge and the remaining half at the right edge. The parameters are $\gamma = 0.5$, $V = 5$, and $N = 90$.

tends to move to one edge. This behavior is distinct from these conventional expectations, adding a unique and interesting aspect to the study of wave dynamics in non-Hermitian physics. To illustrate this, we analyze the spreading dynamics corresponding to an initial single-site excitation of the OBC lattice with $\gamma_R = \gamma_L = \gamma$ and $V = 5$, where the skin states exhibit localization near both edges, i.e., half of the states being localized at the left edge and the remaining half at the right edge. We suppose the initial state at site j and time $t = 0$ is given by $\psi_j(t = 0) = \delta_{j,S}$, where S is the starting site, and then find its time evolution. Figure 4 plots the normalized density $\frac{\psi_j(t)}{\sum_j |\psi_j(t)|^2}$ as a function of time when the initial excitation is close to either the right or left edge. We see that the wave always propagates in the forward direction to the right edge, regardless of its initial excitation location, without experiencing reflection from the right edge. Note that if γ reverses its signs, then the system favors motion towards the left. Additionally, if the next-to-nearest-neighboring couplings are real valued ($\gamma_L \to i\gamma_L$ and $\gamma_R \to -i\gamma_R$), then this asymmetric motion would disappear. This asymmetric motion can be explained as follows. In the absence of losses, $V = 0$, the system has extended eigenstates and the initial wave splits in two and is transported bidirectionally. In the presence of losses with $V = 5$, an imaginary line gap appears, indicating that the skin states localized at the left edge decay much faster than those localized at the opposite edge. Second, the skin states localized at the right edge have shorter localization lengths compared to those at the left edge. As a result, the initial wave splits in two, with the majority of the splitting towards the forward direction. Furthermore, motion in the backward direction is rapidly suppressed, allowing the wave packet to survive and move in the forward direction towards the right edge. This leads to unidirectional wave transport in the lattice, where backward-propagating waves dissipate within a short distance of propagation due to damping.

We have studied the asymmetrical motion, but the question of determining the total dissipated power at each site remains unresolved. Interestingly, in certain cases, we find that most of the initial power is lost not from the starting site, but from the right edge. In the next section, we explore another dynamical phenomena, the so-called non-Hermitian edge burst, to further study this problem.

III. NON-HERMITIAN EDGE BURST IN THE LATTICES WITH BIPOLAR NHSE

Let us study the non-Hermitian edge burst in a lattice with open edges, i.e., $\psi_0 = \psi_{-1} = \psi_{N+1} = \psi_{N+2} = 0$ in Eq. (1). Suppose that the lattice is initially excited at a single site in the bulk near the left edge, described by the initial conditions $\psi_j(t = 0) = \delta_{j,S}$, where the starting site S is an even number. Let $I(t) = \sum_j |\psi_j(t)|^2$ be the total power (norm) with the initial value $I(0) = 1$. Let us multiply Eq. (1) by $\psi_j^\star$ and its complex conjugate by ψ_j, and then subtract these two expressions to obtain $\frac{d|\psi_j|^2}{dt}$. We sum this expression over the index j and, after some algebra, we find that $I(t)$ changes according to

$$\frac{dI}{dt} = -(\gamma_R - \gamma_L) \sum_j \psi_j^\star(\psi_{j+2} + \psi_{j-2}) - 2 \sum_i V_j \, |\psi_j|^2. \tag{5}$$

The first term on the right-hand side of this equation increases the total power and, concurrently, the second term leads to a decrease in the total power. Given the second term's dominance, the initial power is eventually dissipated from the system entirely. Specifically, the power $I(t)$ decays exponentially in time and becomes zero as $t \to \infty$ when $\gamma_R = \gamma_L$. On the contrary, it exhibits either a nonexponential decay or unbounded growth when $\gamma_R \neq \gamma_L$. During nonexponential decay, which occurs when $\gamma_R - \gamma_L$ is sufficiently small, the power $I(t)$ undergoes fluctuations of reduction and growth over time and eventually vanishes. On the other hand, the power grows unboundedly if $\gamma_R - \gamma_L$ is large. Let us integrate the expression Eq. (5) from zero to infinity and assume that $\gamma_R - \gamma_L$ is small enough such that $I(t \to \infty) \to 0$. We define two parameters, the local decay P_j and local growth Q_j probabilities,

$$P_j = 2V_j \int_0^\infty |\psi_j|^2 \, dt,$$
$$Q_j = (\gamma_L - \gamma_R) \int_0^\infty \psi_j^\star(\psi_{j+2} + \psi_{j-2}) \, dt. \tag{6}$$

Note that P_j is nonvanishing only when j is an odd number since losses are not introduced at the even-numbered sites. We obtain the relation between the total dissipated power from the lossy sites and the added power due to the nonreciprocity,

$$\sum_{j=1}^{N} P_j = 1 + \sum_{j=1}^{N} Q_j. \tag{7}$$

This formula is different from the one previously explored in the literature for investigating the non-Hermitian edge burst, where the total dissipated power is equal to the initial power [22–24]. The asymmetrical couplings lead to amplified power. The total extra power $\sum_{j=1}^{N} Q_j$ is ultimately dissipated from the system. Remarkably, the dissipation of this extra power is not uniformly distributed along the lattice. Some lossy sites may experience a more pronounced increase in

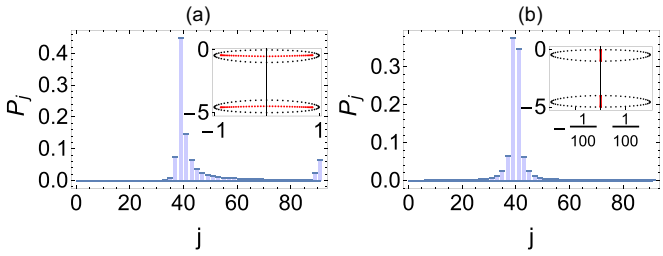

FIG. 5. The distribution of the decay probability P_j: (a) $\gamma = 0.5$ and (b) $\gamma = 1/100$. Both cases exhibit bipolar NHSE with an imaginary line gap of the PBC loops encircling the OBC spectrum on the complex energy plane, where the horizontal and vertical axes are E_R and E_I, respectively (inset). The imaginary gaplessness condition is satisfied by the two systems. However, only the the case in (a) displays the non-Hermitian edge-burst effect $\gg 1$. The parameters are $S = 40$, $N = 91$, and $V = 5$.

dissipated power than others. In some cases, the dissipation of the extra power is predominantly acquired by the right edge, leading to an enhanced edge-burst effect, as shown below.

To study the edge-burst phenomena, we numerically compute the local decay probabilities P_j. To quantify the edge burst, we use the relative height, defined as $P_N/P_{\min}$, where $P_{\min} = \min\{P_S, P_{S+1}, \ldots, P_N\}$ is the minimum of P_j between the starting point S and the right edge. Note that $P_N/P_{\min} \gg 1$ and $P_N/P_{\min} \approx 1$ serve as evidence for the existence and absence of the edge burst, respectively [23]. This condition will be referenced throughout this paper. We can also define another ratio $P_N/P_{S\mp1}$, which compares the decay probabilities at the right edge and the neighboring site of the starting point [24]. This ratio acts as a measure of the strength of the edge burst. We say that the edge-burst effect is strong when this ratio exceeds 1. Below, two distinct cases, one with $\gamma_R = \gamma_L = \gamma$ and the other with $\gamma_R \neq \gamma_L$, are explored.

A. $\gamma_R = \gamma_L = \gamma$

Consider first the system with $\gamma_R = \gamma_L = \gamma$, leading to $Q_j = 0$. In this case, the total power lost from the system equals the initial power. The system is characterized by left-right symmetry and exhibits bipolar NHSE. Therefore, one might intuitively expect that the local decay probability P_j at site j peaks at the neighboring sites of the initially populated site (where the loss rate at $j = S$ is zero) and then decreases exponentially in both directions as one moves away from this site (with j being an odd number). However, this assumption is not accurate. The emergence of a topological funneling effect with a single focal point causes the initial wave to propagate to the right, implying an asymmetric distribution of P_j, leading to bigger losses on the right side of the starting site S than on the left.

Let us now perform numerical computations to examine the P_j distribution. In Fig. 5, we can see the asymmetric P_j distributions. The P_j takes its maximum value near the starting point and rapidly decrease in the bulk towards the edges. Remarkably, a sharp peak occurs at the right edge in the first case, indicating an edge burst, while P_j remain very small near the right edge [see Fig. 5(a)]. The edge burst in this regime is weak as the ratio $P_N/P_{S\mp1}$ is smaller than 1. On the other hand, a similar peak is not observed and the edge burst does not appear in Fig. 5(b), although both cases satisfy the imaginary gap closing condition and exhibit bipolar NHSE, as shown in the insets of Fig. 5. As γ is decreased, it takes more time for the initial excitation to reach the right edge, leading to more losses in the bulk. Consequently, the second system with a very small value of γ does not show the edge-burst effect.

B. $\gamma_R \neq \gamma_L$

The edge-burst effect can be enhanced by amplifying the ratio $P_N/P_{S\mp1}$. This can be achieved by increasing γ while leaving all other parameters fixed. However, the regime of strong edge burst ($P_N/P_{S\mp1} > 1$) is not reachable through this approach. An alternative way is to introduce a small nonreciprocity ($\gamma_R - \gamma_L > 0$). Our approach to finding an instance with a strong edge-burst effect is as follows. We start with a symmetrical system ($\gamma_R = \gamma_L$) already displaying the edge-burst effect and slightly reduce γ_L, while keeping all other parameters unchanged. We remark that a small change of γ_L slightly deforms the PBC loops, preserving the bipolar skin phase. We then employ numerical simulations to investigate whether there is an enhancement in the edge-burst effect. Remarkably, such an enhancement is not primarily attributed to the NHSE, but rather to the asymmetrical power generation that eventually leads to more decay at the right edge than near the starting points. In other words, an asymmetrical distribution of Q_j results in a shift in the P_j distribution, favoring an increased P_N/P_{S+1} ratio. On the other hand, this method has limitations. If the nonreciprocity $\gamma_R - \gamma_L$ is not sufficiently small, the power can grow indefinitely, meaning that P_j also diverge. We therefore consider slight nonreciprocity and sufficiently large V. In this case, the power experiences rapid initial decay, followed by growth after a certain time, ultimately dissipating entirely at large times.

To illustrate our approach, we start with a lattice with $N = 91$, $S = 40$, and $\gamma_R = \gamma_L = 0.2$, and consider two specific cases at $V = 1$ and $V = 4$. First, we confirm that these systems exhibit the weak edge-burst effect with $P_N/P_{S\mp1} < 1$. To enhance the effect, we change γ_L to 0.18 and repeat the numerical calculations with this slight change. Figures 6(a) and 6(b) plot the distribution of local decay probabilities among the whole lattice. Both figures show the enhanced edge-burst effect, with the second one displaying the strong edge-burst effect as $P_N/P_{S\mp1} > 1$. The insets show how the power $I(t)$ changes over time. We see that they experience an exponential decrease, followed by a gradual increase and subsequent decrease, and become practically zero when $t > 300$. Remarkably, the total generated power $\sum_j Q_j$ becomes higher as the loss rate V is larger. Therefore, increasing the non-Hermiticity increase the total generated power. This can enhance the $P_N/P_{S\mp1}$ ratio as the generated power dissipates more at the right edge. Figures 6(c) and 6(d) plot the corresponding Q_j distributions to see the asymmetrical local power generation among the whole lattice. Notably, the entire power generated at the lattice site j does not dissipate exclusively from the same site. The wave packet, experiencing power amplification from asymmetric couplings, moves towards the right edge while concurrently undergoing decay along the way.

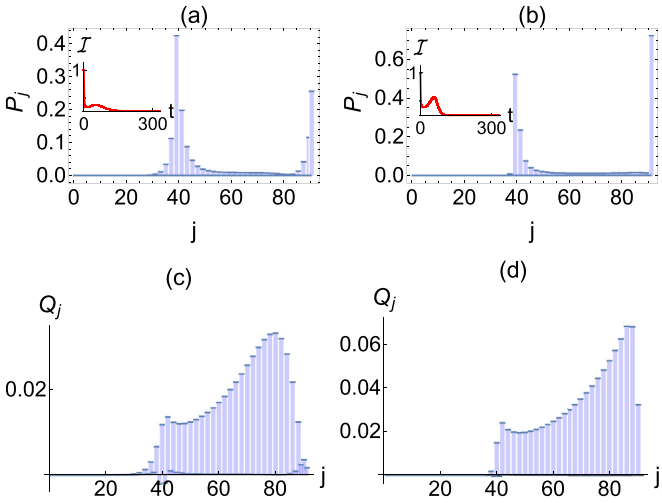

FIG. 6. P_j and the corresponding Q_j at (a),(c) $V = 1$ and (b),(d) $V = 4$. The local decay probabilities P_j at site j exhibit an enhanced non-Hermitian edge-burst effect attributed to nonuniform distribution of the decay of the added power, $\sum_j Q_j$, resulting from the asymmetry in the couplings. (b) Strong edge-burst effect since the ratio $P_N/P_{S\mp1}$ exceeds 1. The insets show the total power $I(t)$ as a function of time. It decays rapidly and then makes a growth before being entirely dissipated. The parameters are $\gamma_L = 0.18$, $\gamma_R = 0.20$, $S = 40$, and $N = 91$.

IV. CONCLUSION

In conclusion, we consider a model featuring a lattice structure with symmetric coupling at nearest neighbors and asymmetric coupling at next-nearest neighbors with losses at alternating sites. Our exploration of the edge-burst phenomenon in a lossy lattice, exhibiting bipolar NHSE, has revealed intriguing dynamics. For the lattice with symmetrical couplings, we observed the coexistence of skin and extended states. Beyond the critical value, a line gap emerged, accompanied by distinct PBC loops encircling OBC eigenvalues. This phenomenon introduces a distinctive behavior in wave propagation.

We explore a topological phase transition from bipolar NHSE to NHSE and calculate the phase transition point V_t for our model. This topological phase transition alters the localization characteristics of the eigenstates. The skin states, localized at both edges, and extended states prior to the phase transition become skin states localized at only one edge after the phase transition occurs.

Our study demonstrated the occurrence of the topological funneling effect with one focal point even in the case of bipolar NHSE. We found that the edge-burst effect manifests, and an asymmetric local decay rate appears, even when the skin states are localized at both edges. To enhance the edge-burst effect, we introduced a slight nonreciprocity in the couplings of a system already exhibiting the edge-burst effect, emphasizing the crucial role of asymmetrical power generation rather than relying solely on NHSE. However, this approach has limitations in achieving a strong edge-burst regime, as the total power may grow unboundedly. The asymmetrical local power generation, as illustrated in the Q_j distributions, significantly contributed to the overall enhanced edge-burst effect. These findings illuminate the rich dynamics and phenomena exhibited by non-Hermitian lattice systems.

The model proposed herein can be experimentally realized in some systems such as electronic and photonic systems, including photonic laser systems. In photonic lattices, asymmetric couplings can be achieved through various engineered structures, including tailored waveguide configurations and coupled resonator arrays [27]. Similarly, in electronic lattices, asymmetric coupling can arise from factors such as lattice distortions and spin-orbit-coupling effects [28]. By leveraging these experimental platforms, our proposed model opens avenues to explore novel dynamical phenomena.

ACKNOWLEDGMENTS

C.Y. wishes to acknowledge the support from the Scientific and Technological Research Council of Turkey (TUBITAK) through the 2501 program with Grant No. 123N121.

[1] S. Yao and Z. Wang, Edge states and topological invariants of non-Hermitian systems, Phys. Rev. Lett. **121**, 086803 (2018).
[2] R. Lin, T. Tai, L. Li, and C. H. Lee, Topological non-Hermitian skin effect, Front. Phys. **18**, 53605 (2023).
[3] C.-X. Guo, C.-H. Liu, X.-M. Zhao, Y. Liu, and S. Chen, Exact solution of non-hermitian systems with generalized boundary conditions: Size-dependent boundary effect and fragility of the skin effect, Phys. Rev. Lett. **127**, 116801 (2021).
[4] L. Li, Ching H. Lee, S. Mu, J. Gong, Critical non-Hermitian skin effect, Nat. Commun. **11**, 5491 (2020).
[5] A. Chakrabarty and S. Datta, Skin effect and dynamical delocalization in non-Hermitian quasicrystals with spin-orbit interaction, Phys. Rev. B **107**, 064305 (2023).
[6] H. Shen, B. Zhen, and L. Fu, Topological band theory for non-Hermitian hamiltonians, Phys. Rev. Lett. **120**, 146402 (2018).
[7] N. Okuma, K. Kawabata, K. Shiozaki, and M. Sato, Topological origin of non-Hermitian skin effects, Phys. Rev. Lett. **124**, 086801 (2020).
[8] K. Zhang, Z. Yang, and C. Fang, Correspondence between winding numbers and skin modes in non-Hermitian systems, Phys. Rev. Lett. **125**, 126402 (2020).
[9] L. Zhang *et al.*, Acoustic non-Hermitian skin effect from twisted winding topology, Nat. Commun. **12**, 6297 (2021).
[10] K. Wang, A. Dutt, K. Y. Yang, C. C. Wojcik, J. Vuckovic, and S. Fan, Generating arbitrary topological windings of a non-Hermitian band, Science **371**, 1240 (2021).
[11] S. M. Rafi-Ul-Islam, Z. B. Siu, H. Sahin, Md. S. H. Razo, and M. B. A. Jalil, Twisted topology of non-Hermitian systems induced by long-range coupling, Phys. Rev. B **109**, 045410 (2024).

[12] W.-C. Jiang, J. Li, Q.-X. Li, and J.-J. Zhu, The reciprocating and bipolar non-Hermitian skin effect engineered by spin-orbit coupling, Appl. Phys. Lett. **123**, 201107 (2023).
[13] L. Eek, A. Moustaj, M. Rontgen, V. Pagneux, V. Achilleos, and C. M. Smith, Emergent non-Hermitian models, Phys. Rev. B **109**, 045122 (2024).
[14] H. Xin, W. Song, S. Wu, Z. Lin, S. Zhu, and T. Li, Manipulating the non-Hermitian skin effect in optical ring resonators, Phys. Rev. B **107**, 165401 (2023).
[15] M.-J. Liao, M.-S. Wei, Z. Lin, J. Xu, and Y. Yang, Non-Hermitian skin effect induced by on-site gain and loss in the optically coupled cavity array, Results Phys. **57**, 107372 (2024).
[16] C.-X. Guo and S. Chen, Exact solutions of non-Hermitian chains with asymmetric long-range hopping under specific boundary conditions, Chin. Phys. B **31**, 010313 (2022).
[17] P. Wen, J. Pi, and G.-L. Long, Investigation of a non-Hermitian edge burst with time-dependent perturbation theory, Phys. Rev. A **109**, 022236 (2024).
[18] S. Ma, H. Lin, and J. Pi, Imaginary gap-closed points and non-Hermitian dynamics in a class of dissipative systems, arXiv:2403.06224.
[19] S. Weidemann, M. Kremer, T. Helbig, T. Hofmann, A. Stegmaier, M. Greiter, R. Thomale, and A. Szameit, Topological funneling of light, Science **368**, 311 (2020).
[20] S. Longhi, Probing non-Hermitian skin effect and non-Bloch phase transitions, Phys. Rev. Res. **1**, 023013 (2019).
[21] C. Yuce, Spontaneous topological pumping in non-Hermitian systems, Phys. Rev. A **99**, 032109 (2019).
[22] L. Wang, Q. Liu, and Y. Zhang, Quantum dynamics on a lossy non-Hermitian lattice, Chin. Phys. B **30**, 020506 (2021).
[23] W.-T. Xue, Y.-M. Hu, F. Song, and Z. Wang, Non-Hermitian edge burst, Phys. Rev. Lett. **128**, 120401 (2022).
[24] C. Yuce and H. Ramezani, Non-Hermitian edge burst without skin localization, Phys. Rev. B **107**, L140302 (2023).
[25] Y.-M. Hu, W.-T. Xue, F. Song, and Z. Wang, Steady-state edge burst: From free-particle systems to interaction-induced phenomena, Phys. Rev. B **108**, 235422 (2023).
[26] L. Xiao, W.-T. Xue, F. Song, Y.-M. Hu, W. Yi, Z. Wang, and P. Xue, Observation of non-Hermitian edge burst in quantum dynamics, arXiv:2303.12831.
[27] C. M. Rechtsman *et al.*, Photonic Floquet topological insulators, Nature (London) **496**, 196 (2013).
[28] S.-Y. Kwon, and C. Zhigang, Photonic crystal lasers ultimate nanolasers, Laser Photon. Rev. **8**, 132 (2014).